Imprints of the Molecular Electronic Structure in the Photoelectron Spectra of Strong-Field Ionized Asymmetric Triatomic Model Molecules

Matthias Paul, Lun Yue, and Stefanie Gräfe*
Institute for Physical Chemistry and Abbe Center for Photonics, Friedrich-Schiller Universität Jena, Helmholtzweg 4, 07743 Jena, Germany

(Received 6 December 2017; published 8 June 2018)

We examine the circular dichroism in the angular distribution of photoelectrons of triatomic model systems ionized by strong-field ionization. Following our recent work on this effect [Paul, Yue, and Gräfe, J. Mod. Opt. **64**, 1104 (2017)], we demonstrate how the symmetry and electronic structure of the system is imprinted into the photoelectron momentum distribution. We use classical trajectories to reveal the origin of the threefolded pattern in the photoelectron momentum distribution, and show how an asymmetric nuclear configuration of the triatomic system effects the photoelectron spectra.

DOI: 10.1103/PhysRevLett.120.233202

Angle-resolved photoelectron spectroscopy has been very successful in probing photoionization and intramolecular dynamics of molecules [1]. The photoelectron angular distributions depend on the symmetry and vibrational dynamics of the probed system, the molecular orbital from which the electron is emitted, the experimental geometry, and the wavelength of the interacting laser pulse. The scattering of the emitted photoelectron off the molecular potential yields the molecular-frame photoelectron angular distribution, which provides rich structure and can be strongly anisotropic. The relative orientation of the molecule to the laser polarization axis or plane strongly determines the shape of the photoelectron angular distributions. Photoelectron angular distributions have been recorded for atoms and molecules interacting with weak [2–4] or intense fields [5–9].

While in the last decades strong-field physics has mainly focused on atoms and small diatomic molecules, also larger and chemically more interesting molecules have moved into the center of research. Many experiments have investigated ionization and fragmentation dynamics of smaller polyatomic molecules in strong laser fields [10–14]. From the theoretical side, it is clear that it is impossible to treat the interaction of polyatomic molecules with intense laser fields fully numerically, as too many degrees of freedom on many different time scales are involved. In addition, in larger systems, many different phenomena such as multielectron or scattering effects may occur. Consequently, the simplest molecules H_2 and H_2^+ have been in the center of theoretical and numerical research [15–21]. They can be regarded as prototype systems, as many effects first detected there have been observed later in larger molecules as well. The molecules H_3^{2+} and H_3^+, the simplest polyatomic molecules, have attracted considerable theoretical interest [22–25]. While also larger nonlinear molecules have been theoretically examined [26–29], most of the work utilized approximations or assumptions to describe the strong-field interaction. On the other hand, a lot of the understanding of strong-field phenomena is based on the strong-field approximation (SFA) [30–32], providing analytical expressions for ionization and photoelectron momentum distributions. In the SFA, it is assumed that the laser field is so strong that after (strong-field) ionization, the electron is solely driven by the laser field and the parent ion represents a small perturbation, which can be neglected. Several attempts have been made to adapt the SFA to molecules to address the additional complications or challenges introduced by the multiatomic center nature of molecules [33–36].

For chiral molecules being ionized by circularly polarized laser pulses, circular dichroism in the photoelectron angular distribution can be observed, with circular dichroism referring to a difference in the interaction of a sample with left- and right-circularly polarized light. However, it has been theoretically predicted [37,38] and later experimentally verified [39,40] that circular dichroism in the photoelectron angular distribution occurs with the sufficient condition of nonplanarity of three vectors defining the experimental system: the propagation axis of the circularly polarized light, the photoelectron momentum, and the molecular axis. Thus, achiral, oriented diatomic molecules can feature circular dichroism in the photoelectron angular distribution. Experimental examples include valence and inner shell photoionization of adsorbed CO molecules [39,40], aligned NO molecules [41–43], and the case of resonant dissociative photoionization of autoionizing H_2 [44].

In this Letter, we extend the investigation towards nonsymmetric, noncolinear molecular systems interacting with intense laser fields. We demonstrate for the first time, to the best of our knowledge, using fully *ab initio* quantum dynamical simulations, how the electronic structure and symmetry of nonlinear triatomic molecules are imprinted

into the photoelectron momentum distribution following strong-field ionization. We are, in particular, interested to analyze which properties of the electronic structure are imprinted into the strong-field photoelectron momentum distribution. For this, we employ our recently developed triatomic model system [45] consisting of a single active electron with two spatial degrees of freedom $\boldsymbol{r} = (x, y)$ interacting with intense, circularly polarized, near- and midinfrared electric fields $\boldsymbol{E}(t)$. The beauty of this model system is that by fine-tuning the charges of the nuclei, we control the symmetry (or its absence). Additionally, we control the range of the potential environment and can investigate which influence the Coulomb potential imprints onto the photoelectron momentum distributions. We analyze the strong-field electron dynamics and the photoelectron momentum distributions by combining different methods, by application of the numerical solution of the time-dependent Schrödinger equation (TDSE), as well as the classical trajectory Monte Carlo (CTMC) and SFA calculations. This enables us to relate the molecular electronic structure to strong-field photoelectron momentum distributions.

The dynamics of the system is governed by the TDSE which reads (atomic units are used unless stated otherwise)

$$\mathrm{i}\frac{\partial}{\partial t}\psi(\boldsymbol{r},t) = \left[-\frac{1}{2}\nabla^2 + V(\boldsymbol{r}) + \boldsymbol{p}\cdot\boldsymbol{A}(t)\right]\psi(\boldsymbol{r},t). \quad (1)$$

In the above equation, the interaction with the external field is given in velocity gauge, with $\boldsymbol{p} = (p_x, p_y)$ the momentum operator and $\boldsymbol{A}(t) = [A_x(t), A_y(t)]$ the vector potential, defined as

$$A_x(t) = \pm\frac{E_0}{\omega} f(t)\sin[\omega(t - t_0) - \phi_{\mathrm{CEP}}],$$
$$A_y(t) = -\frac{E_0}{\omega} f(t)\cos[\omega(t - t_0) - \phi_{\mathrm{CEP}}]. \quad (2)$$

The positive (negative) sign describes right- (left-) circularly polarized (RCP and LCP) fields, E_0 is the field strength, ω the laser frequency, $\phi_{\mathrm{CEP}} = 0$ the carrier-envelope phase, and $t_0 = 0$ fs the time when the Gaussian envelope $f(t)$ is maximum. The model potential $V(\boldsymbol{r}) = V_{nn} + V_{en}(\boldsymbol{r})$ describes bare Coulomb repulsion between the three nuclei V_{nn} with charges Z_i fixed at nuclear positions $\boldsymbol{R}_i$, as well as the interaction of the electron with three nuclei, $V_{en}(\boldsymbol{r})$; see Fig. 1 (a1) and (b1) and the Supplemental Material [46] for details. The positions of the nuclei are set to form an equilateral triangle with internuclear distances between two adjacent nuclei of $R = 3.5$ a.u. The central question of our investigation is to analyze the structure in the photoelectron momentum distributions and how it can be related to the molecular potential. We aim at distinguishing Coulomb effects as originating from excited electronic states and those acting on the continuum electron (long-range contributions).

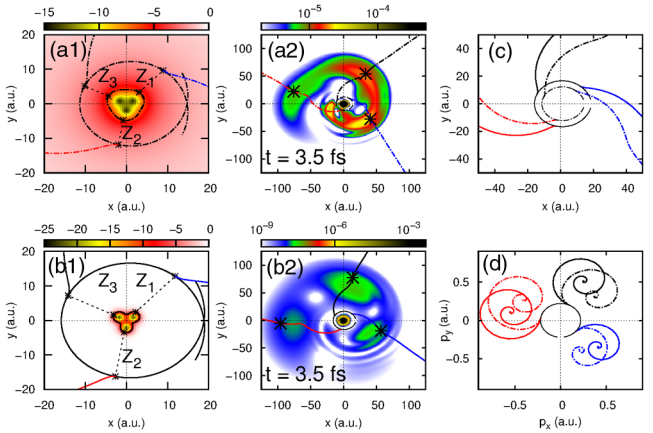

FIG. 1. Comparison of long- and short-range model systems: (a1) Coulombic and (b1) short-range potential (color scale in eV), shifted down to 0. The "circle" around the potential indicates the classical tunnel exits. (a2/b2) Snapshots of the electron density $|\psi(x, y, t_{fix})|^2$ in long-range (a2) and short-range (b2) potentials. The stars indicate the current position of the electron moving along the trajectory. (c),(d) Three selected classical trajectories in coordinate (c) and momentum space (d). The solid lines represent trajectories in the short-range potential, while the dashed lines are trajectories in the Coulomb potential.

We therefore employ potentials of different range to describe the nuclear-electron attraction,

$$V_{en}(\boldsymbol{r}) = -\sum_{i=1}^{3}\frac{Z_i \exp\left(-\beta|\boldsymbol{r} - \boldsymbol{R}_i|^2\right)}{\sqrt{|\boldsymbol{r} - \boldsymbol{R}_i|^2 + \alpha}}, \quad (3)$$

with the softening parameter $\alpha = 1$. The parameter β defines the range of the potential, for $\beta = 0$, the potential is Coulombic. For all cases considered in this work, the nuclear charges Z_i and the short-range parameters β are chosen such that the ionization potential is the same, $I_P = 8.64$ eV (with the specific values being listed in the Supplemental Material [46]). Note that the system is designed such that for the symmetric configuration $Z_1 = Z_2 = Z_3$, the center of mass and charge lies at the origin of the coordinate system, and the system exhibits a mirror symmetry along the y axis.

We numerically integrate the TDSE in Eq. (1) on a 512×512 grid using the split-operator technique [47] and the FFTW 3 library [48]; for details, please refer to Ref. [45] and the Supplemental Material [46]. The photoelectron spectra are obtained by the wave function splitting methods [49,50]. Electronic eigenstates $\varphi_n(\boldsymbol{r})$ are obtained via imaginary time propagation [51]. In all results presented in this work, the initial state is the electronic ground state $\varphi_1(\boldsymbol{r})$.

We compare the results of our *ab inito* quantum dynamics with results obtained by CTMC calculations and the SFA, where after ionization the electron is subjected to the laser field only, completely neglecting the molecular potential. The photoelectron momentum

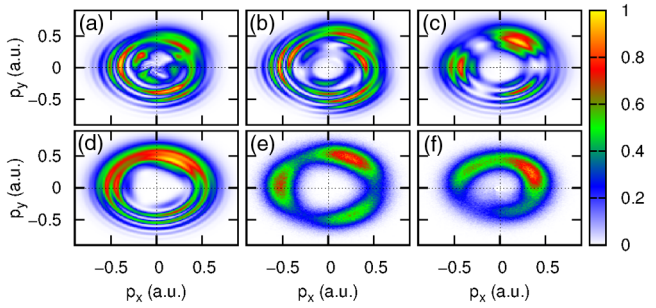

FIG. 2. Photoelectron momentum distributions of the symmetric model system induced by an intense few-cycle LCP laser pulse with $\lambda = 800$ nm, Gaussian full width at half maximum $= 5$ fs, and $E_0 = 0.02$ a.u.. (a) Coulombic potential, (b),(c) short-range potentials ($\beta = 0.005$ and $\beta = 0.3$), (d) short-range SFA, and (e) short-range ($\beta = 0.3$), and (f) long-range CTMC calculations.

distributions $\sigma(\boldsymbol{p})$ are calculated as detailed in the Supplemental Material [46], which contains Refs. [52–54].

We start by investigating the photoelectron momentum distribution of a symmetric model system V_{sym}. Starting from the electronic ground state $\varphi_1(\boldsymbol{r})$, the system interacts with a LCP 800 nm laser pulse with field strength $E_0 =$ 0.02 a.u. and a Gaussian full width at half maximum of 5 fs. This rather intense pulse ionizes the system [17% of the norm of $\psi(\boldsymbol{r}, t)$ leaving the grid], yielding a photoelectron momentum distribution (rescaled to the maximal value) as shown in Fig. 2(a).

It can be seen that the photoelectron momentum distribution originating from the Coulombic system [panel (a)] features the expected above-threshold ionization (ATI) ring structure, together with some groups of prominent signal peaks near $\boldsymbol{p} = (-0.4, 0), \boldsymbol{p} = (0.2, -0.4)$, and some weaker peaks near $\boldsymbol{p} = (0.2, 0.4)$, forming a threefold symmetric structure. Our aim is to assign the observed features of the photoelectron momentum distributions to the structure of the molecular potential and distinguish which features result from contributions of intermediate states and which part can be assigned to the Coulomb character of the continuum. We therefore repeat the calculations with short-range potentials, see Figs. 2(b) and (c). The first prominent difference is that the total ionization yield is reduced substantially (not shown in the figure), the shorter the range of the potential. As in short-range potentials the number of excited states is finite, in contrast to Coulomb-type potentials, and in the limit of true δ potentials reduced to only one single bound state, the multiphoton mechanism of ionization is substantially reduced and ionization proceeds predominantly via tunneling [55,56]. The second difference can be seen at very small momenta: while the Coulombic case shows some fingerlike structure which can be assigned to excited states and multiphoton ionization, these structures are absent for the short-range potentials. The third and most prominent difference of the photoelectron momentum distributions from short-range potentials is that the threefold symmetric peak structure is much more pronounced compared to the Coulombic case. Also shown in Fig. 2 are the results of an SFA calculation, panel (d), and CTMC calculations (see Supplemental Material [46]), panel (e), featuring likewise the threefold symmetric structure.

What is the origin of this threefold structure in the photoelectron momentum distributions? Snapshots of the electronic density (Fig. 2, Supplemental Material [46]) during laser interaction clearly show how the threefold structure is built up during the course of ionization. The origin of the threefold structure during the ionization can be assigned to three different ionization events, reflected by three typical trajectories, see Figs. 1(c) and (d) (solid lines). These trajectories depicted here start with an initial transversal momentum (see Supplemental Material [46]) at tunnel exits located near the nuclei's positions and end up at momenta corresponding to the ones of the short-range quantum dynamical momentum distribution (and also the SFA). We also display the corresponding trajectories for long-range potentials Figs. 1(c) and (d) (dashed lines). It can be clearly seen that the Coulomb continuum causes a pronounced shift to the trajectories, which is, not surprisingly, the strongest at early times, when the electron is close to the nuclear positions. Also, as indicated in Fig. 1, the tunnel exits for the Coulomb potential lie closer to the nucleus than for short-range potentials. Thus, the classical picture suggests that the main influence of the Coulomb continuum is a rotation of the photoelectron momentum distribution. The rotation can also be seen when comparing Figs. 2(a)–(c) and is most pronounced for small momenta (inner ATI rings). This is, however, not all of the differences we can gather if we reconsider Fig. 2(a), as an inner fingerlike structure can be seen. This suggests that the influence of excited states seems to be of importance for the dynamics, as to be expected for strong-field processes with dominant multiphoton character. Still, in order to relate the electronic structure to the photoelectron momentum distributions, in the following discussion, we will thereby focus primarily on short-range potentials, where the influence of excited states is substantially reduced and the overall structure is more pronounced.

We now consider asymmetric potentials. Figure 3 displays the corresponding photoelectron momentum distributions for asymmetric short-range potentials for LCP and RCP pulses. While for the symmetric potential, the change of the polarization direction from LCP to RCP corresponds merely to a mirror image of the photoelectron momentum distribution (reflected on the p_y axis), this is not the case for the asymmetric potentials: these photoelectron momentum distributions differ substantially, as the mirror symmetry in the system is absent. The higher the degree of asymmetry imprinted by the nuclear potential, the less visible becomes the threefold symmetric structure of the photoelectron momentum distributions. At the same time, the intensity pattern of the photoelectron

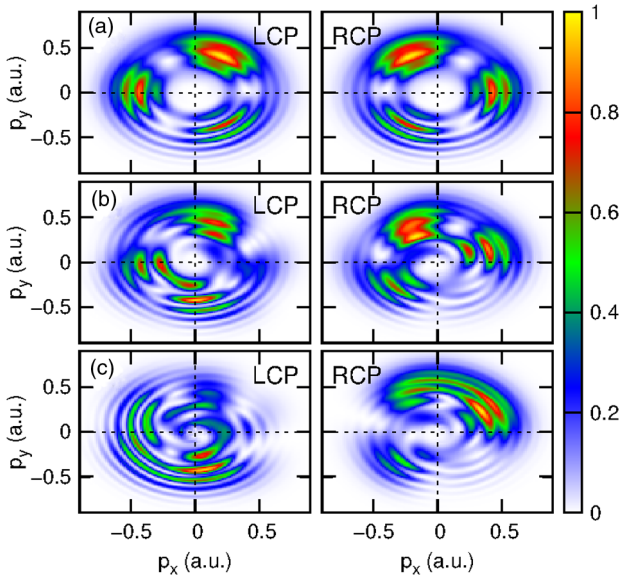

FIG. 3. Photoelectron momentum distributions for LCP (left) and RCP (right) fields for short-range asymmetric potentials. (a) Symmetric case, for comparison. The degree of asymmetry, thus the differences in the charges Z_i of the nuclei, increases from the middle (b) to the lower panels (c). For the corresponding results of the SFA; see Fig. 1, Supplemental Material [46].

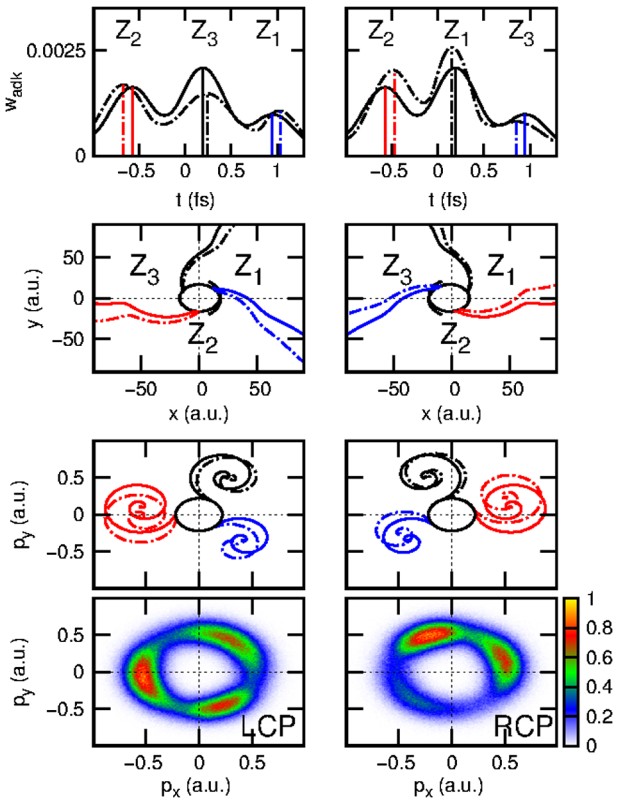

FIG. 4. Overview of the CTMC calculations for the short-range asymmetric potential environment subject to LCP (left column) and RCP (right column) laser fields, respectively. The upper panels display the ionization rate as a function of time for symmetric (solid) and asymmetric potentials (dashed lines). The second and third rows display selected trajectories in coordinate and momentum space. For comparison, also the corresponding trajectories of the symmetric case are displayed (solid lines), while the trajectories for the asymmetric case are represented by dashed lines. The lowest panels show the photoelectron momentum distributions as obtained from the CTMC calculations. Note that the red, blue, and black colors represent representative ionization events.

momentum distributions differ for these few-cycle pulses: while for the LCP pulses, the intense peaks in the photoelectron momentum distributions are located at negative p_y values [$\boldsymbol{p} = (0.1, -0.4)$, third quadrant], the intense peaks for RCP pulses can be seen at positive p_y values [$\boldsymbol{p} = (0.4, 0.2)$, first quadrant], thus causing a strong circular dichroism in the angular distribution.

The reason for this can be understood when considering the classical trajectory picture, see Fig. 4 for LCP and RCP pulses: For LCP, the ionization rate around Z_1 and Z_2 is similar as in the symmetric case, while the ionization rate at times when the electric field vector points in the opposite direction of Z_3 is strongly suppressed. For RCP pulses, ionization around Z_3 behaves similar to the symmetric case, but ionization at times when the electric field vector points in the opposite direction of Z_1 and Z_2 is strongly enhanced; see also Fig. 2 of the Supplemental Material [46]. This results in a strong difference in the intensity pattern. The second difference can be attributed to a difference in ionization times: taking a closer look at the ionization times, we gather that for LCP pulses, ionization around Z_2 happens slightly earlier in asymmetric potentials, while ionization around Z_1 and Z_3 occurs later, leading to a clock- and anticlockwise shift in the photoelectron momentum distributions. For the RCP pulses, the situation differs: ionization around Z_2 happens later for asymmetric potentials, while ionization around Z_1 is almost the same as for symmetric potentials, resulting in an anticlockwise shift in the photoelectron momentum distributions.

To summarize, we have presented results from our *ab initio* quantum dynamical calculations in a two-dimensional, single-active electron model system aiming at answering the question of which information of the molecular electronic structure is imprinted in the photoelectron angular distributions when the system is ionized by intense, few-cycle circularly polarized laser pulses. We have shown that the symmetry of the molecular electronic structure is reflected in the photoelectron momentum distributions, and that Coulomb effects, both due to the presence of excited electronic states and the long-range character of the continuum, are visible in the photoelectron momentum distributions. These Coulomb effects, however, become much less pronounced for longer driving wavelengths; see also the Supplemental Material [46]. In the future, we will expand our investigations towards three-dimensional systems, aiming to describe multiphoton photoelectron circular dichroism occurring in the forward and backward direction with purely *ab initio* calculations. For this, the

results obtained from the calculations in two dimensions and the analysis of different methods in the current simple model system represent an important precursor.

The authors highly acknowledge financial support within the priority programme QUTIF (SPP) from the German Science Foundation (DFG), Grants No. GR 4482/3-1 and No. GR 4482/2-1. S. G. would like to acknowledge fruitful discussions with Professor Manfred Lein and Professor Ulf Saalmann.

*s.graefe@uni-jena.de

[1] K. L. Reid, Annu. Rev. Phys. Chem. **54**, 397 (2003).
[2] M. Yamazaki, J. i. Adachi, T. Teramoto, A. Yagishita, M. Stener, and P. Decleva, J. Phys. B **42**, 051001 (2009).
[3] N. Saito, K. Ueda, A. D. Fanis, K. Kubozuka, M. Machida, I. Koyano, R. Dörner, A. Czasch, L. Schmidt, A. Cassimi, K. Wang, B. Zimmermann, and V. McKoy, J. Phys. B **38**, L277 (2005).
[4] J. Adachi, K. Ito, H. Yoshii, M. Yamazaki, A. Yagishita, M. Stener, and P. Decleva, J. Phys. B **40**, 29 (2007).
[5] M. Wollenhaupt, M. Krug, J. Köhler, T. Bayer, C. Sarpe-Tudoran, and T. Baumert, Appl. Phys. B **95**, 647 (2009).
[6] A. Rouzée, Y. Huismans, F. Kelkensberg, A. Smolkowska, J. H. Jungmann, A. Gijsbertsen, W. K. Siu, G. Gademann, A. Hundertmark, P. Johnsson, and M. J. J. Vrakking, in *Ultrafast Phenomena in Molecular Sciences—Femtosecond Physics and Chemistry*, Spinger Series in Chemical Physics (Springer, New York, 2014), Vol. 107.
[7] L. Holmegaard, J. L. Hansen, L. Kalhoj, S. Louise Kragh, H. Stapelfeldt, F. Filsinger, J. Kupper, G. Meijer, D. Dimitrovski, M. Abu-samha, C. P. J. Martiny, and L. B. Madsen, Nat. Phys. **6**, 428 (2010).
[8] D. Dimitrovski, M. Abu-samha, L. B. Madsen, F. Filsinger, G. Meijer, J. Küpper, L. Holmegaard, L. Kalhøj, J. H. Nielsen, and H. Stapelfeldt, Phys. Rev. A **83**, 023405 (2011).
[9] J. L. Hansen, L. Holmegaard, L. Kalhøj, S. L. Kragh, H. Stapelfeldt, F. Filsinger, G. Meijer, J. Küpper, D. Dimitrovski, M. Abu-samha, C. P. J. Martiny, and L. B. Madsen, Phys. Rev. A **83**, 023406 (2011).
[10] V. R. Bhardwaj, D. M. Rayner, D. M. Villeneuve, and P. B. Corkum, Phys. Rev. Lett. **87**, 253003 (2001).
[11] X. Xie, K. Doblhoff-Dier, S. Roither, M. S. Schöffler, D. Kartashov, H. Xu, T. Rathje, G. G. Paulus, A. Baltuška, S. Gräfe, and M. Kitzler, Phys. Rev. Lett. **109**, 243001 (2012).
[12] X. Xie, K. Doblhoff-Dier, H. Xu, S. Roither, M. S. Schöffler, D. Kartashov, S. Erattupuzha, T. Rathje, G. G. Paulus, K. Yamanouchi, A. Baltuška, S. Gräfe, and M. Kitzler, Phys. Rev. Lett. **112**, 163003 (2014).
[13] X. Xie, S. Roither, M. Schöffler, E. Lötstedt, D. Kartashov, L. Zhang, G. G. Paulus, A. Iwasaki, A. Baltuška, K. Yamanouchi, and M. Kitzler, Phys. Rev. X **4**, 021005 (2014).
[14] B. Wolter, M. G. Pullen, A.-T. Le, M. Baudisch, K. Doblhoff-Dier, A. Senftleben, M. Hemmer, C. D. Schröter, J. Ullrich, T. Pfeifer, R. Moshammer, S. Gräfe, O. Vendrell, C. D. Lin, and J. Biegert, Science **354**, 308 (2016).
[15] T. Zuo and A. D. Bandrauk, Phys. Rev. A **52**, R2511 (1995).
[16] A. Giusti-Suzor, F. H. Mies, L. F. DiMauro, E. Charron, and B. Yang, J. Phys. B **28**, 309 (1995).
[17] T. Kjeldsen, L. Madsen, and J. Hansen, Phys. Rev. A **74**, 035402 (2006).
[18] A. Saenz, Phys. Rev. A **61**, 051402 (2000).
[19] M. Lein, E. Gross, T. Kreibich, and V. Engel, Phys. Rev. A **65**, 033403 (2002).
[20] S. Gräfe and M. Y. Ivanov, Phys. Rev. Lett. **99**, 163603 (2007).
[21] S. Saugout, C. Cornaggia, A. Suzor-Weiner, and E. Charron, Phys. Rev. Lett. **98**, 253003 (2007).
[22] C. Lefebvre, H. Z. Lu, S. Chelkowski, and A. D. Bandrauk, Phys. Rev. A **89**, 023403 (2014).
[23] A. Chen, M. F. Kling, and A. Emmanouilidou, Phys. Rev. A **96**, 033404 (2017).
[24] A. Chen, C. Lazarou, P. H., and A. Emmanouilidou, J. Phys. B **49**, 235001 (2016).
[25] K.-J. Yuan, H. Lu, and A. D. Bandrauk, J. Phys. B **50**, 124004 (2017).
[26] T. K. Kjeldsen, C. Z. Bisgaard, L. B. Madsen, and H. Stapelfeldt, Phys. Rev. A **71**, 013418 (2005).
[27] K. Doblhoff-Dier, M. Kitzler, and S. Gräfe, Phys. Rev. A **94**, 013405 (2016).
[28] A. Russakoff, S. Bubin, X. Xie, S. Erattupuzha, M. Kitzler, and K. Varga, Phys. Rev. A **91**, 023422 (2015).
[29] J. Caillat, J. Zanghellini, M. Kitzler, O. Koch, W. Kreuzer, and A. Scrinzi, Phys. Rev. A **71**, 012712 (2005).
[30] L. V. Keldysh, Zh. Eksp. Teor. Fiz. **47**, 1945 (1964) [Sov. Phys. JETP **20**, 1307 (1965)].
[31] F. H. M. Faisal, J. Phys. B **6**, L89 (1973).
[32] H. R. Reiss, Phys. Rev. A **22**, 1786 (1980).
[33] E. Hasović and D. B. Milošević, Phys. Rev. A **86**, 043429 (2012).
[34] D. B. Milošević, Phys. Rev. A **74**, 063404 (2006).
[35] D. Dimitrovski, C. P. J. Martiny, and L. B. Madsen, Phys. Rev. A **82**, 053404 (2010).
[36] V. I. Usachenko and S.-I. Chu, Phys. Rev. A **71**, 063410 (2005).
[37] N. Cherepkov, Chem. Phys. Lett. **87**, 344 (1982).
[38] R. L. Dubs, S. N. Dixit, and V. McKoy, Phys. Rev. Lett. **54**, 1249 (1985).
[39] C. Westphal, J. Bansmann, M. Getzlaff, and G. Schönhense, Phys. Rev. Lett. **63**, 151 (1989).
[40] C. Westphal, A. P. Kaduwela, C. S. Fadley, and M. A. Van Hove, Phys. Rev. B **50**, 6203 (1994).
[41] K. L. Reid, D. J. Leahy, and R. N. Zare, Phys. Rev. Lett. **68**, 3527 (1992).
[42] T. Jahnke *et al.*, Phys. Rev. Lett. **88**, 073002 (2002).
[43] O. Geßner, Y. Hikosaka, B. Zimmermann, A. Hempelmann, R. R. Lucchese, J. H. D. Eland, P.-M. Guyon, and U. Becker, Phys. Rev. Lett. **88**, 193002 (2002).
[44] D. Dowek, J. F. Pérez-Torres, Y. J. Picard, P. Billaud, C. Elkharrat, J. C. Houver, J. L. Sanz-Vicario, and F. Martín, Phys. Rev. Lett. **104**, 233003 (2010).
[45] M. Paul, L. Yue, and S. Gräfe, J. Mod. Opt. **64**, 1104 (2017).
[46] See Supplemental Material at http://link.aps.org/supplemental/10.1103/PhysRevLett.120.233202 for the model potentials, numerical details, and wavelength dependence of the photoelectron spectra.

[47] M. D. Feit, J. A. Fleck, and A. Steiger, J. Comput. Phys. **47**, 412 (1982).
[48] S. G. J. M. Frigo, ICASSP Conf. Proc. **3**, 1381 (1998).
[49] R. Heather and H. Metiu, J. Chem. Phys. **86**, 5009 (1987).
[50] A. Keller, Phys. Rev. A **52**, 1450 (1995).
[51] R. Kosloff and H. Tal-Ezer, Chem. Phys. Lett. **127**, 223 (1986).
[52] S. V. Popruzhenko, J. Phys. B **47**, 204001 (2014).
[53] J. E. Gentle, *Random Number Generation and Monte Carlo Methods* (Springer, New York, 2003).
[54] N. B. Delone and V. P. Krainov, J. Opt. Soc. Am. B **8**, 1207 (1991).
[55] O. Smirnova, M. Spanner, and M. Y. Ivanov, J. Phys. B **39**, S307 (2006).
[56] S. Gräfe, J. Doose, and J. Burgdörfer, J. Phys. B **45**, 055002 (2012).